Improved Performance of the W7-AS Stellarator with the New Island Divertor

R. Brakel 1), P. Grigull 1), K. McCormick 1), R. Burhenn 1), Y. Feng 1), F. Sardei 1), J. Baldzuhn 1), H. Ehmler 1), F. Gadelmeier 1), L. Giannone 1), D. Hildebrandt 1), K. Ida 2), R. Jaenicke 1), J. Kisslinger 1), T. Klinger 1), J. P. Knauer 1), R. König 1), G. Kühner 1), H. P. Laqua 1), D. Naujoks 1), H. Niedermeyer 1), E. Pasch 1), N. Ramasubramanian 1), N. Rust 1), F. Wagner 1), A. Weller 1), U. Wenzel 1), A. Werner 1), W7-AS Team 1)

1) Max-Planck-Institut für Plasmaphysik, EURATOM Association, D-85748 Garching, Germany

2) National Institute of Fusion Science, 322-6 Oroshi-Cho, Toki, 509-5292 Japan

e-mail contact of main author: brakel@ipp.mpg.de

Abstract: The island divertor concept has successfully been realized at W7-AS. The divertor gives access to a new NBI-heated high density regime with densities up to 4×1020 m-3 and energy confinement well above customary scalings (high density H-mode, HDH). In parallel, impurity confinement dramatically decreases. This prevents impurity accumulation, and allows for quasi-stationary high density discharges with excellent confinement and with radiation profiles peaked at the edge. At the highest densities partial detachment occurs with a radiated power fraction up to 90% at a tolerable mitigation of plasma energy. The HDH-mode appears promising with respect to the requirements of both confinement and exhaust. Major experimental results, such as the lack of a high recycling phase preceding detachment, are also predicted by the EMC3/EIRENE code.

1. Introduction

The island divertor is the natural exhaust concept for the Wendelstein stellarator line. It relies on the field line diversion in magnetic islands, which –for appropriate values of the rotational transform– are inherently formed at the plasma boundary by the finite toroidal periodicity. Recently, Wendelstein 7-AS has been equipped with 10 discrete divertor modules, which in combination with the 5/m-islands (m = 10, 9 or 8; n = 5 is the number of toroidal field periods) constitute the first open island divertor [1]. It serves to explore the general feasibility of the island divertor concept, to gather a data base for the validation of 3-dimensional (3D) island divertor codes under development, and – since basic features resemble those of the forthcoming Wendelstein 7-X divertor – to predict divertor scenarios for W7-X.

The divertor modules with a toroidal extent of 0.7 m are placed at the top and bottom of the elliptically elongated plasma cross sections at the interface planes between the field periods. The standard divertor configuration is characterized by a rotational transform $\iota = 5/9$ at the boundary, a radial and poloidal island width of about 10 and 5 cm respectively, a connection length $L_c \approx 100$ m, a target to x-point distance $\Delta_x \approx 4$ cm, and a minor plasma radius of $a \approx 12$ cm. The small distance between target plate and core plasma necessitates a rather high edge density to efficiently prevent the penetration of recycling neutral particles and impurities into the core. Adequate heating at such densities is provided by NBI.

With the new divertor the plasma performance in W7-AS has improved considerably, and the operational range could be extended to quasi-stationary discharges with very high density and heating power. Even in non-diverted configurations with a smooth last closed magnetic surface the better coverage of the plasma circumference by the divertor targets improved the performance as compared to the previously used limiters. For example, new record β-values,

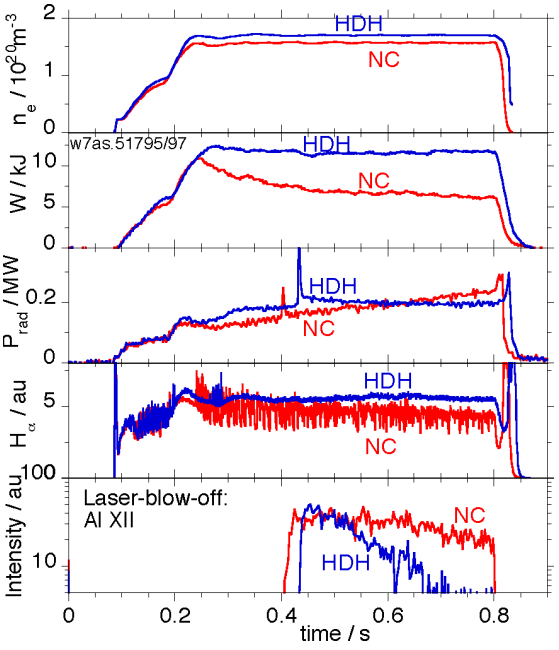

Fig. 1: Two discharges just below (NC = normal confinement) and above (HDH = high density H-mode) the HDH density threshold. The decay curves of laser ablated aluminium clearly demonstrate the reduction of impurity confinement in the HDH-regime. P_{NBI} = 1 MW.

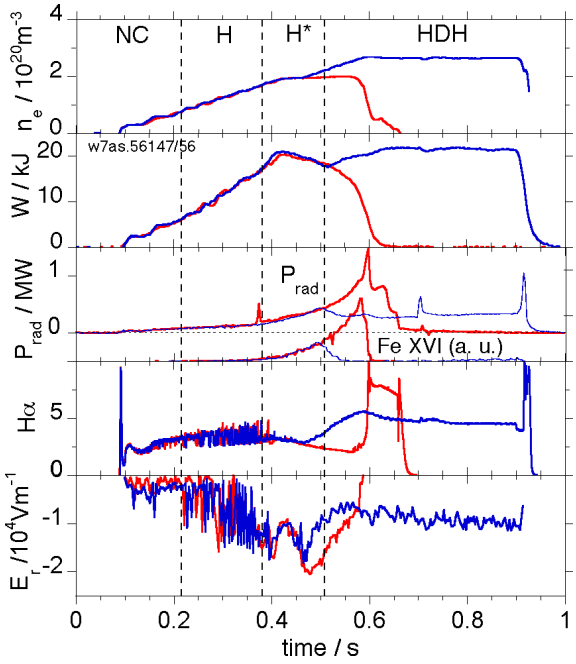

Fig. 2: Density ramp discharges from NC via elmy H-mode to an H*-mode. A density plateau during H* terminates the discharge by impurity accumulation. The collapse is avoided when the density is ramped beyond the HDH-threshold. P_{NBI} = 1.5 MW.

$\langle\beta\rangle \approx 3.4$ %, have been obtained [2]. As a most important result the divertor gives access to a very stable new NBI-heated high density regime with densities up to 4×10^{20} m^{-3} and improved energy confinement well above the customary stellarator scalings [3]. At the highest densities stable detachment can be achieved. The new regime appears very promising with respect to the requirements of both confinement and exhaust.

2. High density operation

With limiters densities beyond 1×10^{20} m^{-3} could be accessed only transiently. The increase of particle and impurity confinement with density caused the loss of density control accompanied with a decrease of temperature and an uncontrollable rise of impurity radiation. This could not be simply overcome by increasing the heating power since beam fuelling and impurity production increased as well. High-density/high-power discharges were terminated by an early radiative collapse [4].

With the divertor density control has improved significantly because of the better coverage of the plasma circumference and the increased pumping capacity of the larger graphite target surface. The length of the density flat top phase could therefore be extended even at high heating power. However, at lower density a long impurity confinement time still leads to a continuous increase of central radiation and the plasma energy settles at normal confinement (NC) levels in terms of the ISS95-scaling [4] (Fig. 1). At higher densities a new regime is encountered, in some features reminiscent of a quiescent H-mode (H*) and therefore being termed “high density H-mode” (HDH): The plasma energy doubles, fluctuations and magnetic activity in the boundary plasma are strongly reduced but, surprisingly, impurity confinement

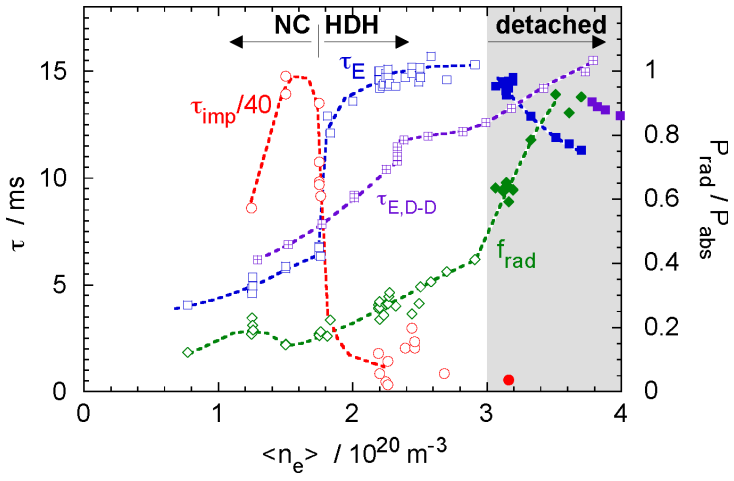

Fig. 3: Dependence of energy confinement time τ_E, impurity confinement time τ_{imp} and radiated power fraction $f_{rad} = P_{rad}/P_{abs}$ on the line averaged density for hydrogen discharges. τ_E is also given for deuterium plasmas (D-D). Full symbols indicate detached discharges. $P_{NBI} = 2$ MW.

dramatically decreases. This prevents impurity accumulation and allows for quasi-stationary conditions. Pulse lengths could be extended beyond $50\times\tau_E$ being limited by the availability of the NBI-sources.

For a given heating power the HDH-mode appears in hydrogen plasmas at a well defined threshold in the line averaged density $\langle n_e \rangle$ as is seen from the density dependence of energy and impurity confinement times (from Al XII, ablated by laser-blow-off (LBO)) in Fig. 3. The threshold density increases with applied NBI power, P_{NBI}, from $\langle n_e \rangle = 1.5\times10^{20}$ m^{-3} at 1.0 MW to 2.2×10^{20} m^{-3} at 3.5 MW. The transition from NC to HDH is more gradual in deuterium. At the entrance into HDH the plasma radiation typically amounts to a fraction $f_{rad} = P_{rad}/P_{abs} \approx$ 30% of the absorbed heating power, P_{abs}. The radiation continues to rise smoothly until it reaches values $f_{rad} \approx 40\%$ where the plasma begins to detach from the targets. At the onset of detachment f_{rad} jumps to $\approx$ 60% and the plasma energy starts to decrease slightly. At the highest densities f_{rad} reaches 90% with a respective reduction of the target power load. Access to a stable HDH-mode is very robust against changes in the magnetic configuration, but stable divertor detachment requires that island size and x-point to target distance are sufficiently large. By decreasing the island size or moving the x-point towards the target, i.e. by approaching a limiter configuration, an oscillating radiation instability occurs.

The HDH-mode is reliably obtained in a fast density ramp with strong gas puffing like in Fig. 1. A slow ramp leads to a radiative collapse by impurity accumulation while passing through NC, or the H*-mode –having a lower density threshold– may occur prior to the HDH-mode in configurations where both improved regimes can exist as in Fig. 2 (here, deviating from the standard divertor configuration, $\Delta_x \approx 1.3$ cm and a ≈ 13.6 cm, which is favourable for the H-mode). The two discharges in Fig. 2 clearly illustrate the different dynamics of the NC-, H*- and HDH-regime, respectively. Both discharges enter the H*-mode after passing through NC and elmy H-mode during a slow density ramp. In one case, the density is kept constant after the H*-transition and enhanced impurity accumulation terminates the discharge within $\approx 5\tau_E$. In the other case the collapse is prevented by ramping the density after a short plateau beyond

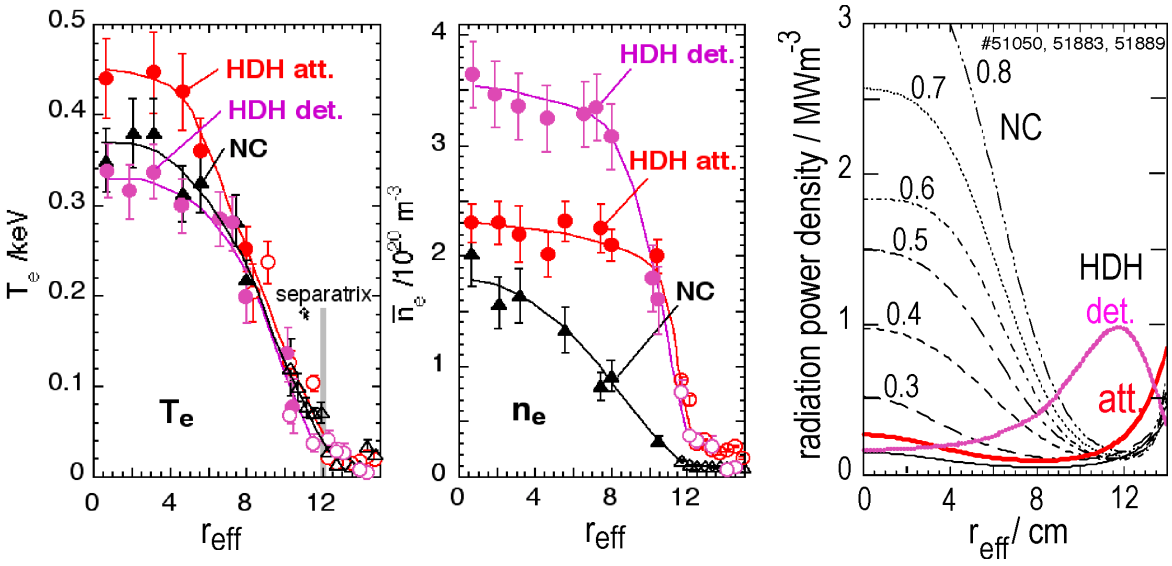

Fig. 4: Radial profiles of temperature, density and radiation power density for normal confinement (NC), attached (HDH att.) and detached (HDH det.) high density H-mode. $P_{NBI} = 2$ MW.

the HDH-threshold. When HDH is accessed accumulation immediately stops, radiation decreases and quasi-stationary conditions can be established. Although impurity confinement is totally different, energy confinement in HDH and H* is comparable. The initial NC-phase exhibits a high H_α-fluctuation level, followed by an elmy phase. In the H*-phase the edge is very quiescent at low H_α-level. At the H*-HDH transition H_α increases but the fluctuation level remains rather low. Mirnov coil data show the same signatures for the magnetic activity (not shown). The value of the radial electric field close to the separatrix, measured by passive B IV spectroscopy, is about 2x higher in the H*- than in the HDH-mode.

The gain in plasma energy of the HDH-mode over normal confinement is due to the drastic change of the density profile: the previously peaked profile becomes flat, the upstream density at the separatrix, n_{es}, increases strongly and a steep density gradient develops at the edge. In contrast, the temperature profile retains its shape and the central values improve slightly (Fig. 4). Within resolution and accuracy of the Thomson scattering systems the density and temperature profiles are very similar for HDH- and H* mode. The radiation profiles are centrally peaked for NC and H* and increase in time whereas they are stationary and flat or peaked at the edge in the attached HDH-regime [6]. The radiation zone moves inward with the onset of detachment.

3. Density limit

The extension of the operational range by the divertor is visualized in Fig. 5, which compares the density limit with the values predicted from the empirical scaling

$$\langle n_e \rangle_{DL} = 1.462\ (P/V)^{0.48}\ B^{0.54}\ (10^{20} m^{-3})$$

obtained from previous limiter discharges. P(MW) is the absorbed heating power, V(m^3) the plasma volume and B(T) the magnetic field strength. The density limit for a particular configuration and heating power is determined as the line-averaged density value where in a

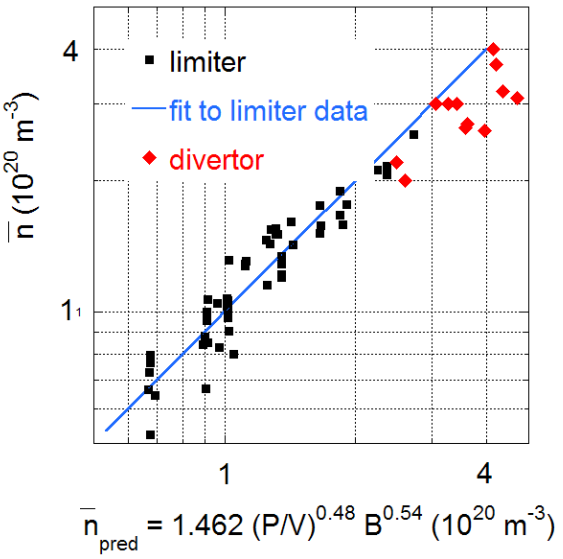

Fig. 5: Achieved versus predicted density limit values for limiter and divertor discharges. The predicted scaling has been obtained from the limiter case.

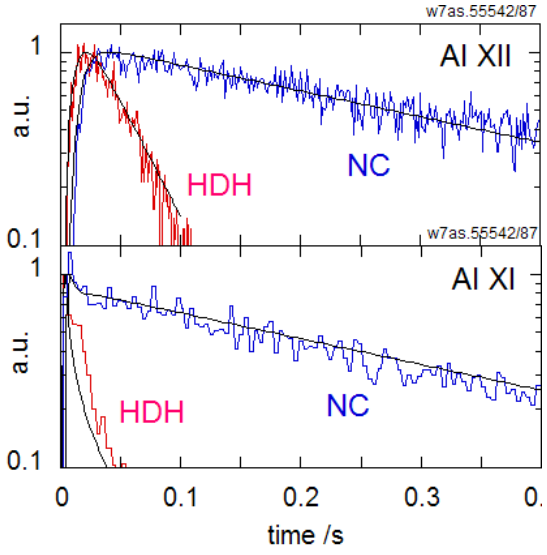

Fig. 6: Aluminium ablation traces for NC- and HDH-discharges compared with simulations by the impurity transport code SITAR. P_{NBI} = 1 MW.

slow density ramp confinement significantly starts to degrade (threshold to radiation collapse with limiter, onset of detachment with divertor). The limiter data base covers the parameter range P_{NBI} = 0.5 – 2.0 MW and B = 1.25 – 2.5 T. The discharges are not stationary but show a steady degradation of plasma energy. The highest density is 2.5×10^{20} m^{-3} at P_{NBI} = 2 MW [4]. Discharges at higher power are extremely transient and not considered. With divertor the maximum densities that can be attained surpass those from limiter discharges by a factor of about 2 for two reasons: (i) the discharges are much less affected by core impurity radiation and (ii) improved density control allows the use of the full available NBI power under quasi-stationary conditions. The highest density achieved under attached conditions is 4×10^{20} m^{-3} at 4 MW whereas 3×10^{20} m^{-3} is reached at 2 MW. The latter value is not much higher than for the limiter case, however, it is obtained under stable quasi-stationary conditions.

4. Impurity transport

Low impurity confinement in the HDH regime is clearly related to a strong reduction of the inward impurity pinch [7]. Time traces of spectral line intensities from LBO-injected aluminium are reasonably simulated by a simplified transport model assuming a constant diffusion coefficient D_{imp} and an inward pinch velocity $v_{imp} = (r/a)\ v_a$ which linearly increases towards the edge (Fig. 6). Both NC and HDH discharges are well described by the same diffusivity (D_{imp} = 0.07 (0.12) m^2/s at 1 (2) MW heating power), whereas the inward pinch has to be strongly reduced for HDH (v_a = – 0 (2.5) m/s) as compared to NC (v_a = – 6 (10) m/s).

This behaviour is in parts consistent with neoclassical impurity transport considerations. The impurities are deep in the collisional regime whereas background ions (H^+) in the core are marginally in the plateau regime ($\nu^* \approx 0.2$) and collisional at the edge. Under these conditions and with peaked ion density profile n_i the inward directed impurity flux $\propto \nabla n_i$ dominates over the outward flux $\propto \nabla T_i$ and the diffusive flux $\propto \nabla n_{imp}$. This leads to accumulation with long confinement times and centrally peaked radiation profiles and is consistent with the observations in NC. For the HDH-mode with flat n_i-profile the flux $\propto \nabla n_i$ vanishes in the

centre, such that ∇T_i drives the impurities outward ("temperature screening"). Since the impurity sources are localized at the edge hollow impurity and radiation profiles result, consistent with the observations in HDH. However, the steep density gradient at the edge is neoclassically expected to drive a locally strong inward pinch which represents a "bottleneck" for the escape of impurities from the plasma. In contradiction to the experiment long confinement times τ_{imp} would result. This qualitative picture is confirmed by preliminary SITAR-code calculations. The contradiction can be resolved for example by assuming an additional increase of the impurity diffusivity at the edge [7]. Code simulations indicate a very high sensitivity of τ_{imp} to width and position of the region with enhanced diffusion. This may play a role in the totally different impurity confinement in HDH- and H*-mode, although the background profiles seem to be only marginally different.

5. Physics of detachment

A realistic modelling of plasma transport in the complex 3D-geometry of an island divertor, including a selfconsistent treatment of impurity transport, has become possible by the EMC3-EIRENE code [8]. Figure 7 shows remarkable agreement between the calculated relation of downstream and upstream density, n_{ed} and n_{es}, and the results of an experimental density scan at 2 MW launched NBI power, covering the range $\langle n_e \rangle = 0.8$ to 3.8×10^{20} m^{-3}. n_{es} and the power into the SOL, $P_{SOL} = P_{abs} - P_{rad,core}$, are input to the code and have been adapted to the experimental data. Due to radiation from the core P_{SOL} is strongly reduced with respect to the absorbed heating power when the density is increased. Initially, n_{ed} linearly increases up to 4×10^{19} m^{-3} with n_{es}, but when P_{SOL} is not sufficient to sustain ionization in front of the targets the ionization front gradually shifts towards the separatrix and n_{ed} decreases at constant $n_{es} = 6\times10^{19}$ m^{-3} (density rollover, note that P_{SOL} decreases further). Finally, when the impurity radiation capability in front of the targets exceeds P_{SOL} the radiation zone jumps to the separatrix (onset of detachment). Consistent with the experimental results, the code predicts detachment for an island divertor to occur at rather high upstream density and high-recycling is not observed in any phase, i.e. the downstream density is always smaller than the upstream

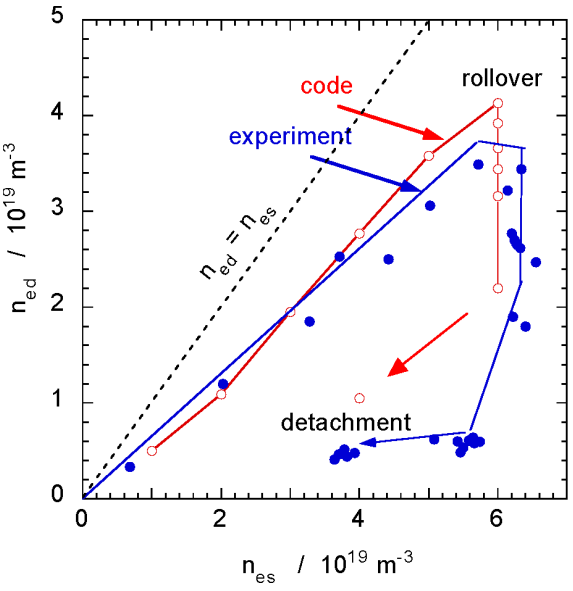

Fig. 7: Downstream versus upstream density from an experimental density scan at 2 MW applied NBI power and from a simulation with the EMC3/Eirene code.

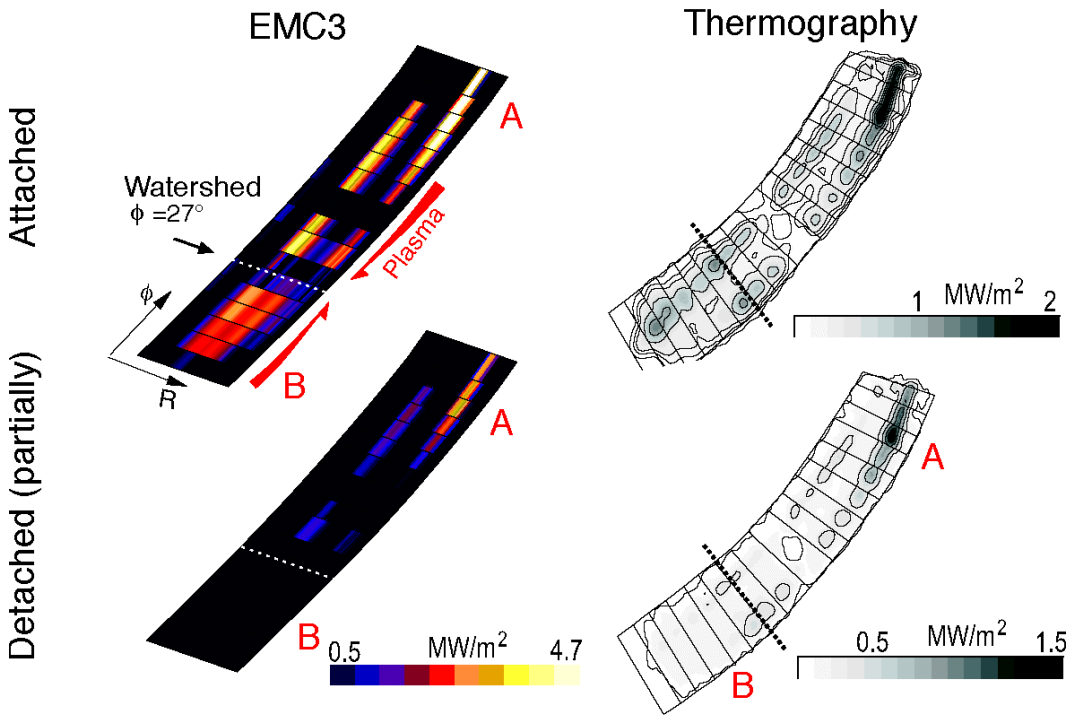

Fig. 8: Power deposition pattern on a target plate for attached and detached situations as observed by thermography (right) and the simulation by EMC3/Eirene (left). The "watershed" separates the target areas which are connected by the field lines with the outboard (A) and inboard (B) side of the torus.

density. This is in evident contrast to the tokamak poloidal-field divertor and is due to the particular geometry of the island divertor. The field-line pitch in the island reference frame is very small and consequently, the connection length L_c between stagnation point and target plate is very large. Furthermore, the distance of the x-point to the target plate is much smaller than in tokamak divertors. As a result, perpendicular transport in the scrape-off layer (SOL) is much more important than in tokamaks. The loss of parallel momentum via cross field transport causes the pressure to drop towards the targets already at low density/high temperature where CX-losses are not effective [8]. It should be mentioned that prior to the density rollover the experimental upstream temperature and pressure already start to decrease. This may additionally support the onset of detachment.

Structural details observed in the target load pattern can be reproduced by the code as well. As an example the power load pattern measured by thermography for attached and detached conditions is compared with the simulation in Fig. 8. In the attached case the pattern can be understood from the footprints of the island fans intersected by the target. In the detached case the plasma remains attached to the target in the region A ("partial" detachment). An explanation is given by the code. Topologically, regions A and B are separated by a watershed such that the field lines connect A with the outboard and B with the inboard side of the torus, respectively. At the outboard side the perpendicular heat flux across the separatrix into the SOL is larger due to flux compression whereas on the inboard side the impurity radiation (from carbon) is higher due to lower temperature. Both effects lead to a higher parallel heat flux within the SOL to region A which therefore remains attached.

6. Discussion

With the island divertor a new quality of high-power/high-density NBI discharges has been achieved in W7-AS. Compared with the previous limiter configuration the operational space of quasi-stationary discharges has been substantially extended with respect to pulse length, density and heating power. The reasons are twofold: improved density and impurity control even at lower density (NC-regime) and, at higher density, the occurrence of the HDH-mode with simultaneously high energy and low impurity confinement. There are indirect indications, e.g. a higher gas puff rate to sustain the same density, that bulk particle confinement in HDH may be reduced as well.

A consistent understanding of the HDH-mode has not yet emerged. A quasi-coherent MHD-mode as in the enhanced D_α H-mode in Alcator C-Mod [9] is not observed. Energy confinement, plasma profiles and – at least for configurations where both modes can exist – a low fluctuation level at the edge are similar to the quiescent H-mode, whereas impurities behave completely different. The hollow radiation profiles in HDH are consistent with "temperature screening" of highly collisional impurities in a marginal collisionless ion background. However, the small impurity confinement time is not explained by purely neoclassical arguments, since the strong density gradient at the edge forms a transport barrier for impurities. The hypothetical enhancement of impurity diffusion at the edge would resolve this contradiction and might help to explain the different impurity behaviour in H* (peaked radiation profiles, long τ_{imp}). A key question concerns the appearance of HDH at lower collisionality, which however can hardly be assessed in W7-AS since the threshold density and thus ν^* increase with power. Furthermore, a selfconsistent picture of the NC-HDH transition has to include the role of the particle sources, which shift from central fuelling by beam deposition in NC to edge fuelling by gas puff and recycling in HDH.

The HDH-mode gives easy access to island divertor relevant edge densities over a wide range of island configurations and heating power, making the W7-AS divertor an ideal test-bed for 3D island divertor theory and modelling. The experimentally observed lack of a high recycling phase preceding detachment has been predicted by the EMC3/EIRENE code. It emphasises the importance of cross field transport as the result of the rather large connection lengths in the SOL. Structural details of particle and power deposition patterns on the targets can be explained by the code to result from inboard/outboard asymmetries due to flux compression. Further details can be attributed to ExB drift effects [10]. The large data base which has been gathered will be extremely useful for code validation and extrapolation to W7-X divertor scenarios.

References

[1] P. Grigull et al., Plasma Phys. Contr. Fusion **43**, A175 (2001)
[2] A. Weller et al., 19th IAEA Fusion Energy Conference, Lyon (2002)
[3] K. McCormick et al., Phys. Rev. Lett. **89**, 015001 (2002)
[4] L. Giannone et al., Plasma Phys. Control. Fusion **42**, 603 (2000)
[5] U. Stroth et al., Nucl. Fusion **36**, 1063 (1996)
[6] L. Giannone et al., Plasma Phys. Control. Fusion **44**, 2149 (2002)
[7] R. Burhenn et al., 29th EPS Conference Montreux, ECA **26B**, P-4.043 (2002)
[8] Y. Feng et al., Plasma Phys. Contr. Fusion **44**, 611 (2002)
[9] J. Snipes et al., Plasma Phys. Contr. Fusion **43**, L23 (2001)
[10] Y. Feng et al., Proc. 15th PSI Conference, Gifu, (2002), to be published in J. Nucl. Mater.